平成２４年度　厚生労働科学研究費補助金
（創薬基盤推進研究事業（政策創薬探索研究事業））
分担研究報告書

複数の作用メカニズムを同時に発現する革新的抗がん剤の開発

研究代表者：椎名　勇（東京理科大学理学部教授）

分担研究課題名：リダイフェン相互作用タンパク質同定解析に関する研究

研究分担者：長谷川　慎（長浜バイオ大学バイオサイエンス学部准教授）

研究要旨

リダイフェンのプロテアソームへの阻害作用に関し、相互作用タンパク質の結合様式を明らかにした。プロテアソームは細胞周期・がん抑制・遺伝子転写など多様な機能調節タンパク質の選択的分解に関わっているプロテアーゼ複合体である。その阻害剤は、細胞周期の停止や増殖因子発現の抑制など複合的作用をもたらし、がん細胞をアポトーシスへと導くことから、新しいクラスのがん分子標的薬として期待されている。体内動態やコストの点で、リダイフェンのような非ペプチド基本骨格の阻害剤は、大きな優位性が期待できる。

A．研究目的

本研究では新規化合物リダイフェン(RID) の抗がん作用メカニズムと分子構造に基づく分子間作用の詳細を明らかにすることを目的とする。昨年度に引き続き、RIDの化学構造、プロテアソーム阻害作用、抗がん作用の3者の関係を検証した。

プロテアソームの担うタンパク質分解機構は、恒常性の維持や細胞の増殖や代謝といった様々な細胞内プロセスの制御において重要な役割を担っている。プロテアソームが適切なタイミングで特定のタンパク質を分解することにより、細胞周期制御やシグナル伝達、免疫応答、アポトーシスなどを適切に制御している。このような生理機能に基づき、プロテアソーム阻害剤は、抗がん剤としての強い作用があり、実用化もされている。その代表例が、ボルテゾミブ（PS-341、商品名：ベルケード）である。ボルテゾミブの開発はミレニアム・ファーマスーティカルズ社により進められ、治療抵抗性の多発性骨髄腫を対象として、2003年に米国で、次いで 2006 年に本邦でも認可された。次世代分子標的抗がん剤として、副作用の少なく体内動態に優れたプロテアソーム阻害剤の開発が期待されている。

RID は、3 成分連結反応によるタモキシフェン合成法から派生する誘導体であり、図１の構造式中 R1 および R2 部位に多様性を持つフォーカストケミカルライブラリーを形成する一群の化合物である。

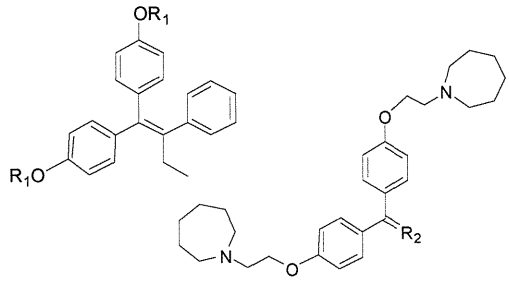

図１　RID 構造多様性導入部位

タモキシフェンは乳がん細胞において抗エストロゲン作用を発揮する化合物であり、乳がんの治療薬として広く用いられている。タモキシフェンはエストロゲン受容体に結合することにより、エストロゲンとエストロゲン受容体の結合を阻害し、がん細胞の増殖を抑制する。ところが、興味深いことに RID はエストロゲン受容体の発現していないがん細胞にも増殖抑制効果がある。本研究では、この作用がプロテアソーム阻害に基づくものであることについて仮説を得て、多くのエビデンスを蓄積してきた。これらを踏まえ、RID の構造活性相関を明らかにすることで、究極的には次世代抗がん剤のドラッグデザインを目指す。

B．研究方法

精製 20S プロテアソーム活性中心の親和性標識に対する保護効果：活性中心を親和性標識するケミカルプローブとして、biotin-belactosin A はプロテアソーム活性中心へ共有結合形成し、ビオチン検出試薬によりブロット膜上の標識タンパク質バンドを検出することができる（Hasegawa et al. Bioorg. Med. Chem. Lett., 18, 5668）。化合物の添加により、この標識から保護されることは、化合物がプロテアソームの基質結合部位に可逆的拮抗阻害様式で作用することを示す。

また、得られた結果について、統合計算科学システム MOE によるドッキングシミュレーションにより考察した。

（倫理面への配慮）

すべての実験は、長浜バイオ大学の各種規程に従い実施した。この基準に照らして、今年度の実施項目について倫理面に問題ないと判断した。

C．研究結果

一群のリダイフェン F（RID-F）構造置換体のプロテアソーム阻害活性を詳細に検討した結果、阻害作用に重要な部位、その構造要件、阻害様式を明らかにした。タモキシフェン自体にはプロテアソーム阻害作用は見出されなかった一方で、その誘導体について比較的強い阻害作用が見出された。次に、細胞レベルでの作用とプロテアソーム阻害との関連性を示した。そして、計算機シミュレーションにより結合様式について考察した。

D．考察

これらの実験データを基礎として、統合計算科学システム MOE を用いプロテアソームの基質結合ポケットに対する RID 化合物群のドッキングシミュレーションを行った。このプログラムでは、タンパク質表面の窪みを探索し、そこに親水性または疎水性の仮想原子を配置、これら仮想原子クラスターに対して最も適合する薬剤立体配置を選択する。基質結合部位に RID が結合することは、今年度の研究結果により証明されたことから、タンパク質表面の探索領域を限定でき、精度の高い予測が得られるものと考えられた。

解析の結果、RID-F の基質結合ポケットへの結合様式について、プロテアソームの酵素サブユニットの活性中心を形成する基質結合ポケットに直接相互作用するという仮説が得られた（図２）。この相互作用モデルでは、RID 化合物群の構造の中で、プロテアソームへの結合部位は２か所存在す

ることである。すなわち、図１の RID-F の化学構造において R1 部位のホモピペリジン環、R2 部位のビニールベンゼンが、プロテアソームの基質結合ポケットに作用するちょうど良い形状を持っており、この部位がそれぞれ結合する 2 種類の結合モードの存在が示唆された。

このような結果から、RID の特定部位に関して、系統的に置換基を導入して阻害活性との相関を明らかにすることで、薬剤の改良に資する基礎データが得られたものと考えられる。

今年度は、これらの検証のほか、培養細胞に RID 化合物群を添加し、アポトーシス誘導の検証をおこなった。この検証については来年度も継続し、RID 化合物群の抗がん作用の詳細を明らかにする予定である。

G．研究発表

１．論文発表

投稿中

２．学会発表

日本ケミカルバイオロジー学会第 8 回年会「新規タモキシフェン誘導体リダイフェン-F に見出されたプロテアソーム阻害作用の構造活性相関研究」長谷川慎 1)、○田中誠 1)、安田ゆかり 1)、塩生真史 1)、佐々木隆造 1)、水上民夫 1)、中田健也 2)、梅田絵梨 2)、王エンブン 2)、渡邊千尋 2)、植竹祥子 2)、椎名勇 2)（2013 年 6 月 19 日発表予定）

H．知的財産の出願・登録状況
（予定も含む。）

１．特許取得

検討中

２．実用新案登録

なし

３．その他

なし

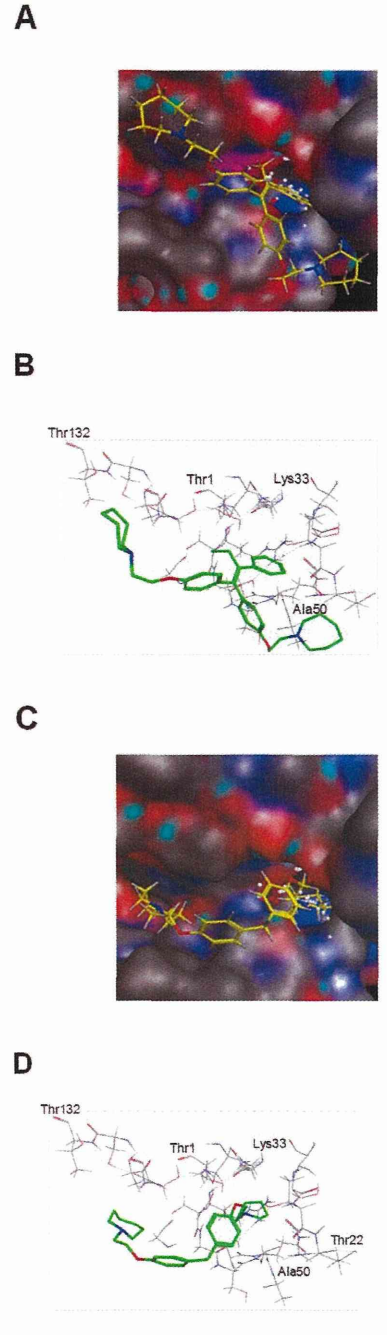

図２　（A）・（B）結合様式①：R2 部位がプロテアソーム（β1）の活性中心に作用。
（C）・（D）結合様式②：R1 部位がプロテアソーム（β1）の活性中心に作用。

平成２４年度　厚生労働科学研究費補助金
（創薬基盤推進研究事業（政策創薬探索研究事業））
分担研究報告書

複数の作用メカニズムを同時に発現する革新的抗がん剤の開発

研究代表者：椎名　勇（東京理科大学理学部教授）

分担研究課題名：抗Ｃ型肝炎ウイルス活性評価に関する研究

研究分担者：深澤秀輔（国立感染症研究所　真菌部　室長）

研究要旨
HCV JFH1株をHuh7.5.1細胞に感染させる系を用い、ウイルスRNAの定量RT-PCR、細胞増殖阻害の解除の測定、細胞内Coreタンパク質のcell-based ELISA等、HCVの全生活環を標的にする抗HCV薬スクリーニング系を確立した。抗HCV活性の評価を行い、ridaifensに抗HCV活性が確認された。ridaifensの抗HCV活性は、主にウイルスの侵入過程の阻害によることが推定されたが、複製等の後期過程にも作用ことが示された。

Ａ．研究目的

変異を起こして耐性になりやすいウイルスの治療には多様な標的を持つ抗ウイルス剤が必要とされる。Huh7.5.1細胞－JFH1の感染系を用いて、C型肝炎ウイルス（HCV）治療薬開発のための探索系を確立し、侵入過程や粒子の放出過程を含む、HCVの全ライフサイクルを標的とするスクリーニングを行い、抗HCV薬の候補物質を探索、得られた活性物質の作用を解析し、HCV生活環の理解、治療薬開発へと発展させる。

Ｂ．研究方法

抗HCV薬スクリーニング系の構築

HCV JFH1株をHuh7.5.1細胞に感染させる系を用いて、放出されたウイルス粒子をPCRチューブに吸着させ、one-step real-time RT-PCRを行いウイルスRNAを定量する系（Antiviral Research 83:112-117, 2009)、HCVによる細胞増殖阻害効果の解除を指標とする系（Biol Pharmaceut Bull 35:1320-1327, 2012)、cell-based ELISAにより細胞内のHCV Core蛋白質を定量する系を開発した。構築した系を用い、種々化合物の抗HCV作用を評価し、その作用機序を解析した。

（倫理面への配慮）

培養細胞を使った研究であり、倫理面への配慮は特に必要ない。

Ｃ．研究結果

抗HCV薬の候補物質を探索するために３種類のアッセイ系を構築し、選択的エストロゲン受容体モジュレーター（Selective estrogen receptor modulator; SERM)を中心に、種々の化合物の抗HCV活性を調べた。Ridaifensと構造が類似の、triphenylethyleneを基本骨格に持つtamoxifen、clomifene、hydroxytamoxifene はHCV複製を強く阻害し、ウイルスRNA産生の50%阻害濃度は約0.1 μMであった。細胞毒性が観察される濃度は、HCV阻害濃度の100倍以上（＞10 μM）であった。ま

たraloxifeneもほぼ同じ強さの阻害効果を示した。

SERMsの阻害過程を特定するため、薬剤添加の時間がHCV阻害効果に及ぼす影響を培地中のHCV RNA RT-PCRアッセイによって解析した。HCV-JFH1の生活環はHuh7.5.1細胞中では約48時間で完了する。感染時より48時間10 μM のtamoxifenが存在すると、培地中に放出されるHCV RNA量は98%減少した。HCVの細胞への侵入は、2時間程度で完了すると考えられるが、tamoxifenを最初の2時間だけ作用させた後、培地を交換してtamoxifenを除いてもほぼ同等のHCV阻害効果が観察されたことから、tamoxifenはHCVの侵入過程を阻害していることが示唆された。しかし感染2時間後、すなわちHCVが細胞に侵入した後からtamoxifenを作用させた場合でも、48時間後の培地中のHCV RNAは90%減少、24時間後から作用させても40%減少したことから、tamoxifenはHCV侵入後の過程も阻害することが示された。SERMsのHCV侵入過程に対する影響をさらに調べるために、HCV疑似粒子(pseudo-particle) (HCVpp)を用いた解析を行うと、阻害が観察され、侵入過程に作用していることが確かめられた。水疱性口内炎ウイルス疑似粒子 (vesicular stomatitis virus) の侵入に対する作用はほとんどなく、SERMsはある程度の選択性を持ってHCVを阻害することが分かった。侵入後の過程に対する作用を調べるため、genotype 2aおよび1bのsubgenomic replicon細胞のウイルスRNA、タンパク質の量を測定した。阻害濃度は10 μM以上とそれほど強くはなかったが、tamoxifenと clomifeneの阻害効果は確認された。

RidaifensはSERMsと類似したHCV阻害作用を示した。HCV-JFH1株をMOI=2でHuh7.5.1細胞に感染させると、細胞増殖はコントロールの5%程度に低下するが、RID-PAが0.5 μM存在すると細胞増殖は50%にまで回復した。RID-PA自体の細胞増殖抑制効果は0.5 μMでは観察されず、5 μMでも約25%であった。RID-PAは感染2時間後に加えた場合、増殖抑制を回復させる効果は低下したことから、SERMs同様、侵入を含む初期の過程を阻害することが示唆された。しかし、HCV NS5Aのタンパク質量を調べると、感染4時間後に加えても阻害が観察され、ウイルス侵入後のステップにも作用していると考えられた。またgenotype 1bのfull genomic replicon、2aのsubgenomic replicon細胞に作用させ、ウイルスタンパク質のレベルを調べるとやはり減少しており、侵入以外の過程も阻害することが明らかとなった

D．考察

ウイルスRNAの定量RT-PCR、細胞増殖阻害の解除の測定、細胞内Coreタンパク質のcell-based ELISA等、HCVの全生活環を標的にする抗HCV薬スクリーニング系を確立した。RID-PAはこれらのアッセイ系でHCV阻害活性を示した。その主たる作用点は、現時点では侵入過程を含むHCV生活環の比較的早い段階であると推定されるが、tamoxifen等のSERMsと同様、より後期の過程にも作用していると考えられる。RID-PA以外にもいくつかのridaifensが抗HCV作用を示した。細胞毒性が弱い(IC50＞10 μM) ものとしては、RID-A、RID-B、RID-PD、RID-PE等が、細胞毒性は比較的強いが、低濃度でHCV複製を阻害するものとしてはRID-E、RID-PC、RID-PG等があげられる。ridaifens、SERMsの抗HCV活性とERに対する作用には今のところ明確な相関は見られない。ERがHCVの複製に必要な宿主因子であるかどうか、今後その他のridaifensの作用を調べることによって明らかにできることが期待される。

E．結論

HCVの全生活環を標的とした抗HCV薬スクリー

ニング系を構築し、抗HCV活性の評価を行った。ridaifensはtamoxifen等のSERMs同様、HCV生活環の複数の過程を阻害すると考えられた。Ridaifensは、HCV生活環を理解するための有用なツール、さらにはHCV治療薬へ発展することが期待される。

G．研究発表

1．論文発表

Murakami, Y., Fukasawa, M., Kaneko, Y., Suzuki, T., Wakita, T., Fukazawa, H. Selective estrogen receptor modulators inhibit hepatitis C virus infection at multiple steps of the virus lifecycle. Microbes and Infection 15:45-55, 2013

Fukazawa H, Suzuki T, Wakita T, Murakami, Y. A Cell-Based, Microplate Colorimetric Screen Identifies 7,8-Benzoflavone and Green Tea Gallate Catechins as Inhibitors of the Hepatitis C Virus. Biological and Pharmaceutical Bulletin 35:1320-1327, 2012

H．知的財産の出願・登録状況

なし

別紙４

研究成果の刊行に関する一覧表

書籍

著者氏名	論文タイトル名	書籍全体の編集者名	書　籍　名	出版社名	出版地	出版年	ページ
矢守隆夫，上原至雅，深澤秀輔，吉田稔，井本正哉，清宮啓之，馬島哲夫，水上民夫，川田学，長田裕之，旦慎吾，松浦正明，掛谷秀昭，冨田章弘.	特集・制がん剤の分子標的スクリーニング成績「化学療法基盤情報支援班」報告-制がん候補物質のスクリーニング成績・第15報-	化学療法基盤情報支援班	癌と化学療法	癌と化学療法社	東京	2013	印刷中

雑誌

発表者氏名	論文タイトル名	発表誌名	巻号	ページ	出版年
Senko Tsukuda, Tomoe Kusayanagi, Eri Umeda, Chihiro Watanabe, Yu-ta Tosaki, Shinji Kamisuki, Toshifumi Takeuchi, Yoichi Takakusagi, Isamu Shiina, Fumio Sugawara	Ridaifen B, a Tamoxifen Derivative, Directly Binds to Grb10 Interacting GYF Protein 2	Bioorganic & Medicinal Chemistry	21 (1)	311-320	2013
Isamu Shiina, Yuma Umezaki, Yoshimi Ohashi, Yuta Yamazaki, Shingo Dan, Takao Yamori	Total Synthesis of AMF-26, an Antitumor Agent for Inhibition of the Golgi System, Targeting ADP-Ribosylation Factor 1	Journal of Medicinal Chemistry	56(1)	150-159	2013
Wen-zhi Guo, Yanwen Wang, Eri Umeda, Isamu Shiina, Shingo Dan, Takao Yamori	Search for Novel Anti-tumor Agents from Ridaifens Using JFCR39, a Panel of Human Cancer Cell Lines	Biological and Pharmaceutical Bulletin	DOI: 10.1248/bpb.13-00129	印刷中	2013
Midori Takeyoshi, Seiya Sakemoto, Isamu Shiina, Kenya Nakata, Keiko Fujimori, Yanwen Wang, Eri Umeda, Chihiro Watanabe, Shoko Uetake, Takao Yamori, Shingo Dan, Yoji Yoshimi, Takahisa Shinomiya, Masahiko Ikekita	Novel Tamoxifen Derivative Ridaifen-B Induces Bcl-2 Independent Autophagy without Estrogen Receptor Involvement	Biochemical and Biophysical Research Communications	DOI: 10.1016/j-bbrc.2013.05.040	印刷中	2013

（作成上の留意事項）
１．省略
２．「５．研究成果の刊行に関する一覧表」に記入した書籍又は雑誌は、その刊行物又は別刷り一部を添付すること。
３．「１．厚生労働科学研究費補助金研究報告書表紙」から「５．研究成果の刊行に関する一覧表」までの報告書等、及び「５．研究成果の刊行に関する一覧表」に記入した書籍又は雑誌の刊行物又は別刷りは、一括して製本すること。ただし、一冊に製本することが困難な場合は複数の分冊ごとに製本することとし、各々の分冊に表紙を付けるとともに分冊の番号（１／ｎ冊、２／ｎ冊、一等)を表示すること。
４．研究報告書（当該報告書に含まれる文献等を含む。以下本留意事項において同じ。）は、国立国会図書館及び厚生労働省図書館並びに国立保健医療科学院ホームページにおいて公表されるものであること。
５．研究者等は当該報告書を提出した時点で、公表について承諾したものとすること。
６．その他
日本工業規格Ａ列４番の用紙を用いること。各項目の記入量に応じて、適宜、欄を引き伸ばして差し支えない。

Bioorganic & Medicinal Chemistry 21 (2013) 311–320

Contents lists available at SciVerse ScienceDirect

Bioorganic & Medicinal Chemistry

journal homepage: www.elsevier.com/locate/bmc

Ridaifen B, a tamoxifen derivative, directly binds to Grb10 interacting GYF protein 2

Senko Tsukuda [a], Tomoe Kusayanagi [a], Eri Umeda [b], Chihiro Watanabe [b], Yu-ta Tosaki [b], Shinji Kamisuki [a], Toshifumi Takeuchi [a], Yoichi Takakusagi [a], Isamu Shiina [b], Fumio Sugawara [a,*]

[a] Department of Applied Biological Science, Faculty of Science and Technology, Tokyo University of Science, 2641 Yamazaki, Noda, Chiba 278-8510, Japan
[b] Department of Applied Chemistry, Faculty of Science, Tokyo University of Science, 1-3 Kagurazaka, Shinjuku-ku, Tokyo 162-8601, Japan

ARTICLE INFO

Article history:
Received 31 August 2012
Revised 3 October 2012
Accepted 5 October 2012
Available online 29 October 2012

Keywords:
Ridaifen B
Tamoxifen
Phage display
GIGYF2
Akt

ABSTRACT

Ridaifen B (RID-B) is a tamoxifen derivative that potently inhibits breast tumor growth. RID-B was reported to show anti-proliferating activity for a variety of estrogen receptor (ER)-positive human cancer cells. Interestingly, RID-B was also reported to possess higher potency than that of tamoxifen even for some ER-negative cells, suggesting an ER-independent mechanism of action. In this study, a T7 phage display screen and subsequent binding analyses have identified Grb10 interacting GYF protein 2 (GIGYF2) as a RID-B-binding protein. Using a cell-based assay, the Akt phosphorylation level mediated by GIGYF2 was found to have decreased in the presence of RID-B.

1. Introduction

Tamoxifen (Fig. 1) is an antagonist of the estrogen receptor (ER) and is widely used in hormone therapy and to prevent the recurrence of cancer in patients with ER-positive breast cancers.[1,2] In breast cancer cells, tamoxifen inhibits cell proliferation by blocking growth signals and inducing apoptosis.[3] However, recent reports have shown that tamoxifen induces apoptosis even in ER-negative cells, which suggests that tamoxifen has other target proteins.[4,5] Additionally, tamoxifen can induce some major side effects including a higher incidence of endometrial cancer and drug resistance following long-term therapy.[6,7] In our previous studies we synthesized novel tamoxifen derivatives in order to better understand the mechanism of action of this drug and to generate new therapeutic agents with reduced side effects.[8,9]

Ridaifen B (RID-B), one of these tamoxifen derivatives (Fig. 1), showed a higher inhibitory activity on cellular proliferation than that of tamoxifen. The global anti-tumor activity of RID-B against a variety of human cancer cells showed that RID-B displayed no difference in inhibitory activity between ER-positive and ER-negative cells.[9,10] Furthermore, on an analysis using a COMPARE program, it was suggested that the mode of action for RID-B was different from that for more than 200 of existing drugs for cancer treatment including tamoxifen.[9] These data indicated that there may be an unknown ER-independent mode of action for RID-B.

To identify RID-B-binding proteins, we used a T7 phage display method. Phage display is a powerful technique for identifying peptides or proteins that bind to proteins or small molecules of interest. However, unlike protein samples, passive immobilization of

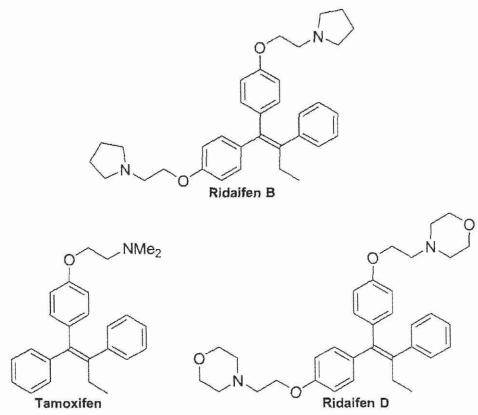

Figure 1. Chemical structures of tamoxifen, RID-B and RID-D.

* Corresponding author. Tel.: +81 471 24 1501x3400; fax: +81 471 23 9767.
E-mail address: sugawara@rs.noda.tus.ac.jp (F. Sugawara).

0968-0896/$ - see front matter © 2012 Elsevier Ltd. All rights reserved.
http://dx.doi.org/10.1016/j.bmc.2012.10.037

small molecules onto a plate surface is generally unsuccessful. Therefore, biotinylated small molecule derivatives and avidin-coated microplates are universally used for affinity selection. A T7 phage display method uses a library constructed from T7 phage particles. Each phage particle expresses peptides of up to about 1200 amino acids in length on the capsid that is identical to proteins or their fragments encoded in living cells or organs.[11–13] Through several rounds of screening, phage particles displaying amino acid sequences that recognize the small molecule of interest are gradually enriched. The amino acid sequences expressed on the capsid of the selected phage particles are then easily identified by sequencing the phage DNA. A subsequent similarity search in the genome database enables a prediction of the potential binding partner(s) as well as the likely binding site. Moreover, unlike many other methods, phage display does not rely on the target protein being soluble and expressed at relatively high levels. Thus, phage display facilitates the identification of less soluble proteins, such as membrane proteins, as well as proteins with a low expression level. In the past several years, we have determined a number of binding partners of small molecules by using a T7 phage display screening protocol.[14–20]

Here we report the identification of Grb10 interacting GYF protein 2 (GIGYF2) as a RID-B-binding protein using a T7 phage display screen. It has been demonstrated that GIGYF2 regulates phosphatidylinositol-3-kinase (PI3K)/Akt signaling pathway of the receptor tyrosine kinase, which is involved in cell proliferation.[21,21] A bead pull-down assay and surface plasmon resonance (SPR) analyses confirmed the direct interaction between RID-B and GIGYF2. Furthermore, using a cell-based assay, the Akt phosphorylation level mediated by GIGYF2 was found to have decreased in the presence of RID-B. These results might explain a possible ER-independent mode of action for RID-B.

2. Results and discussion

2.1. Synthesis of biotinylated RID-B and ridaifen D derivatives

Biotinylated RID-B (Bio-RID-B), 2-[3-(*N*-biotinyl-6-aminohexanoyl)phenyl]-1,1-bis{4-[2-(pyrrolidin-1-yl)ethoxy]phenyl}-1-butene (**7**), was synthesized by the Mukaiyama reductive coupling reaction,[23,24] and the Shiina esterification,[25–27] as shown in Scheme 1. First, 1-[3-(benzyloxy)phenyl]propanone (**2**)[28] was treated with an excess amount of 4,4′-dihydroxybenzophenone (**1**) in the presence of the low-valent titanium species generated from titanium(IV) chloride with zinc powder to afford the desired cross coupling product **3** in 94% yield. The phenol moieties in **3** were transformed into the corresponding aminoethyl ethers by alkylation in 88% yield, and the benzyl protective group in the tetrasubstituted olefin **4** was then cleaved under hydrogenation conditions to provide the phenol derivative **5** in 92% yield. Finally, rapid esterification of *N*-biotinyl-6-aminohexanoic acid (**6**) with the RID-B derivative **5** was carried out in dimethylformamide (DMF) solvent using 2-methyl-6-nitrobenzoic anhydride (MNBA) with 4-(dimethylamino)pyridine (DMAP). The facile dehydration process successfully furnished the probe molecule **7** in 70% yield. It is noteworthy that this is the first application of the MNBA-mediated

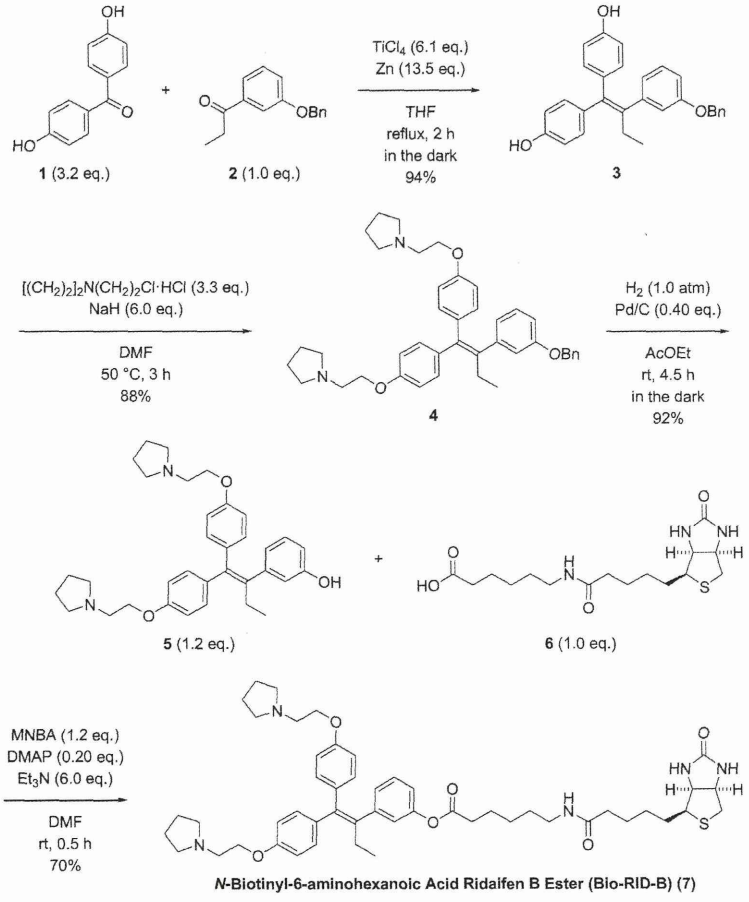

Scheme 1. Synthesis of a biotinylated RID-B derivative (Bio-RID-B) (**7**).

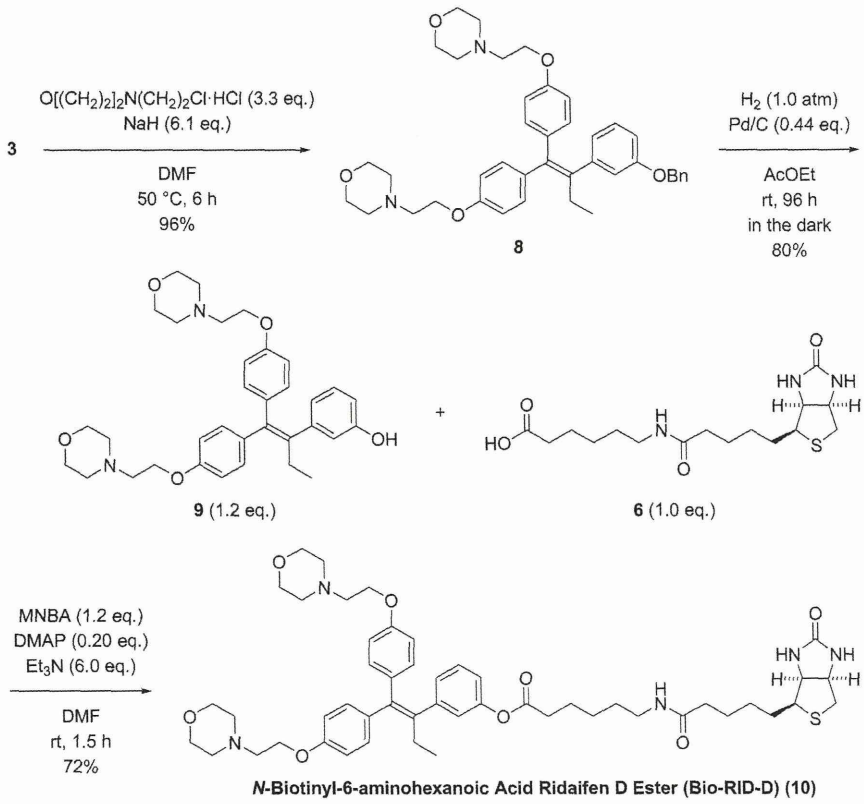

Scheme 2. *Synthesis of a biotinylated RID-D derivative (Bio-RID-D) (**10**).*

coupling reaction between carboxylic acids and alcohols to the expeditious and effective synthesis of the biotin labeled small molecules.[29,30]

Next, biotinylated RID-D (Bio-RID-D), 2-[3-(*N*-biotinyl-6-aminohexanoyl)phenyl]-1,1-bis{4-[2-(morpholin-4-yl)ethoxy]phenyl}-1-butene (**10**), was also synthesized using a similar procedure as described in Scheme 2. Aminoethyl groups were introduced into the bisphenol **3** in 96% yield, and the phenol derivative **9** was successively prepared from the benzyl ether **8** by hydrogenation in 80% yield. Facile esterification of **6** with the RID-D derivative **9** also took place in the presence of MNBA and DMAP to afford the probe molecule **10** in 72% yield.

2.2. Selection of RID-B-binding protein using a T7 phage display screen

To explore RID-B-binding proteins, we performed a phage display screen. A T7 phage library was constructed from a cDNA library of Jurkat cells, an estrogen receptor-negative human leukemia cell line. First, the T7 phage library was incubated with Bio-RID-B immobilized on streptavidin-coated wells. After incubation, unbound and non-specifically bound phage particles were removed by washing. Finally, the remaining phage particles on the wells were eluted and amplified for the next round. The ratio of recovered phage titer dramatically increased after four rounds of selection, indicating the enrichment of T7 phage particles that potentially bind to RID-B (Fig. 2A). Fifteen individual phage plaques were randomly isolated after the fourth round of selection and the amino acid sequence of the displayed protein was determined. Three out of the 15 phage clones had the same DNA sequence encoding a polypeptide of 286 a.a., whereas the remaining 12 phage clones encoded a polypeptide of 135 a.a. (Table 1). We also

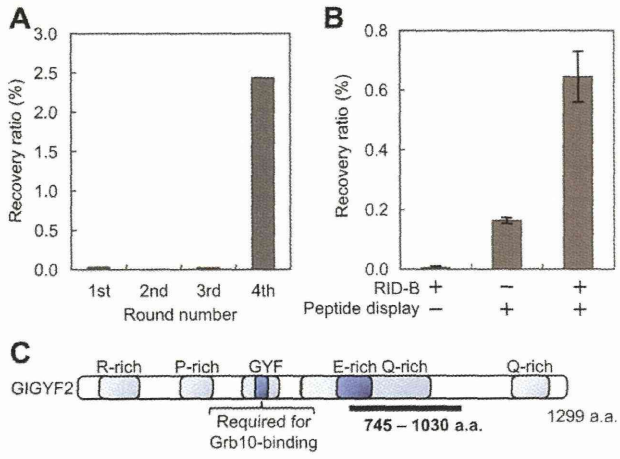

Figure 2. Selection of RID-B-binding protein by a T7 phage display screening procedure. (A) Relative enrichment of T7 phage particles binding to RID-B in each round of selection. The phage titer in the eluate from the Bio-RID-B-immobilized well was compared to the input library titer and shown as recovery ratio. (B) Affinity check of the 286 a.a. phage clone for RID-B. The T7 phage that displays the 286 a.a. [peptide display (+)] or control phage clone [peptide display (−)] was incubated in a well with [RID-B (+)] or without [RID-B (−)] of Bio-RID-B and shown as recovery ratio (%). (C) Schematic representation of full-length GIGYF2. Underline indicates the region that corresponds to the 286 a.a. sequence displayed on the RID-B-binding T7 phage clone.

performed the screening of clones that bind to ridaifen D (RID-D) (Fig. 1), whose cytotoxic activities are lower than that of RID-B, as well as a screen for clones that bind nonspecifically to the control well containing no immobilized small molecule. We obtained two

Table 1
Amino acid sequences and frequency of the phage clones selected from the Bio-RID-B immobilized well

Amino acid sequence	Number of amino acid	Frequency
DPSKGRWVEGITSEGYHYYYDLISGASQWEKPEGFQGDLKKTAVKTVWVEGLSEDGFTYYYNTETGE SRWEKPDDFIPHTSDLPSSKVNENSLGTLDESKSSDSHSDSDGEQEAEEGGVSTETEKPKIKFKEKNK	135	12/15
EMRAKREEEERKRQEELRRQQEEILRRQQEEERKRREEEELARRKQEEALRRQREQEIALRRQREEEERQQQEEA LRRLEERRREEEERRKQEELLRKQEEEAAKWAREEEEAQRRLEENRLRMEEEAARLRHEEEERKRKELEVQR QKELMRQRQQQQEALRRLQQQQQQQQQLAQMKLPSSSTWGQQSNTTAEMRAKREEEERKRQEELRRQQE EILRRQQEEERKRREEEELARRKQEEALRRQREQEIALRRQREEEERQQQEEALRRLEERRREEEERRK	286	3/15

After the fourth-round of selection by T7 phage display, 15 single phage clones were randomly picked and their DNA sequences analyzed to determine the phage displayed peptides.

clones from the Bio-RID-D-immobilized well and two clones from the control well. The phage clone displaying a polypeptide of 135 a.a. was observed in the eluate from the control well in addition to the RID-B and RID-D immobilized wells, suggesting this was a nonspecific binding phage clone (Tables 1, S1 and S2).

We decided to check the affinity of the T7 phage displaying the 286 a.a. polypeptide for RID-B. The corresponding T7 phage clone and a control T7 phage clone displaying no peptide were amplified and then separately added to the RID-B-immobilized well or a blank control well. The bound T7 phage particles were then recovered and the ratio of the two phage clones isolated from the RID-B-immobilized well was compared to that from the non-immobilized control well. The recovery ratio of the phage clone displaying the 286 a.a. polypeptide was four-fold higher from the RID-B immobilized well than from the blank control well. Furthermore, the control phage clone did not bind to RID-B. These results indicated that the phage clone displaying the 286 a.a. polypeptide selectively interacts with RID-B (Fig. 2B).

A similarity search using FASTA identified that the 286 a.a. sequence displayed on the RID-B-binding phage clone is identical to the 745–1030 region of Grb10 interacting GYF protein 2 (GIGYF2) (Figs. 2C and S1). It has been reported that GIGYF2 is a protein that interacts with growth factor receptor-bound protein 10 (Grb10) and has a critical role in the PI3K/Akt signaling pathway. However, its molecular function is not fully understood. Despite the high molecular weight of GIGYF2 (1299 a.a.), use of T7 phage display and subsequent similarity search enabled the identification of this protein as a potential RID-B-binding partner along with a candidate binding site in 745–1030. This 286 a.a. sequence did not show any similarity with GIGYF1, an another subtype of GIGYF, indicating that binding of RID-B to GIGYF is specific for subtype2.

2.3. Interaction analysis between RID-B and GIGYF2

To confirm the interaction between GIGYF2 and RID-B, we performed a pull-down assay. Flag-tagged GIGYF2 was transiently expressed in HEK-293T cells (Fig. 3A), and the cellular lysates were incubated with Bio-RID-B- or biotin-immobilized resin. The bound proteins were then analyzed by Western blotting using an antibody against GIGYF2. Flag-tagged GIGYF2 was found to bind to Bio-RID-B-immobilized resin, but not to the control resin (Fig. 3B). We further elucidated the interaction and estimated the dissociation constant (K_D) between GIGYF2 and RID-B using surface plasmon resonance (SPR) analysis. We engineered a His-tagged truncated form of GIGYF2 corresponding to the 745–1030 region of GIGYF2 (GIGYF2(745–1030)) that is, the region displayed on the RID-B-binding phage (Fig. 3A and C). The recombinant protein was then purified to homogeneity. Various concentrations of GIGYF2(745–1030) were injected over the surface of the SA sensor chip on which Bio-RID-B had been immobilized through the interaction between biotin and avidin. GIGYF2(745–1030) bound to RID-B in a dose-dependent manner and global fitting gave a K_D value of 186 nM. These results indicate that RID-B strongly interacts with the 745–1030 a.a. region in GIGYF2 (Fig. 3D).

We also compared the affinity of the ridaifen analogs for GIGYF2. Previously, we synthesized several ridaifen derivatives and found that the cytotoxic activity of the ridaifen derivatives was dependent on its side chain.[8,9] Among them, RID-D ($\mathrm{Log}GI_{50}$ = −4.84 M) containing morpholine side chains showed low cytotoxicity with non-apoptotic activity in contrast to RID-B ($\mathrm{Log}GI_{50}$ = −5.93 M). In addition, no phage clone displaying GIGYF2 was acquired from a T7 phage display screen using Bio-RID-D (Table S1). Therefore, we speculated that the binding affinity between GIGYF2 and RID-D was less than that for RID-B. As shown in Figure 3B, we attempted the pull-down assay using Bio-RID-D and found that Bio-RID-B-immobilized resin bound to Flag-tagged GIGYF2 more strongly than Bio-RID-D-immobilized resin. Furthermore, SPR analysis showed that RID-B binds to GIGYF2(745–1030) at the range of concentrations tested (Fig. 3D and E). By contrast, little response was observed for RID-D, which is consistent with the results from the pull-down assay (Fig. 3F). Thus, the affinity of each ridaifen derivative for GIGYF2 correlated with the cytotoxicity data.

2.4. Effect of RID-B on the PI3K/Akt signaling pathway

Previous reports indicated that *GIGYF2* was a candidate gene for PARK11-linked Parkinson's disease. Furthermore, recent studies have reported the involvement of GIGYF2 in the PI3K/Akt signaling pathway,[21,22,31] and GIGYF2 was shown to be up-regulated in breast cancer cells in which high phosphorylation levels of Akt are observed. Thus we reasoned that the binding of RID-B to GIGYF2 might be biologically relevant. Initially, we examined whether RID-B affects the phosphorylation level of Akt. HEK293T cells transiently-expressing GIGYF2 were cultured in serum-free medium following pretreatment with RID-B for 4 h, and then stimulated with IGF-1 at different times. The phosphorylation of Akt at Ser473, which is known to be a representative marker for activation of Akt,[32–34] was detected by Western blot analysis using anti-phospho-Akt (Ser473) antibodies. As shown in Figure 4, the phosphorylation level of Akt at Ser473 15 min after IGF-1 stimulation was significantly reduced by RID-B in a dose-dependent manner. By contrast, there was no reduction in the phosphorylation level of Akt when the experiment was conducted using cells transfected with mock empty vector.

Taken together, our results demonstrate that RID-B directly binds to GIGYF2 and reduces the phosphorylation level of Akt at Ser473. This is the first report of a small molecule that binds to GIGYF2 to inhibit its function. Indeed, the knockdown of GIGYF2 reduced cell proliferation in breast cancer cell lines,[31] the RID-B-GIGYF2 interaction and subsequent inhibitory effect of the Akt phosphorylation may be relevant to the anti-proliferative activity of RID-B as well. Further experiments will clarify the detailed mode of actions.

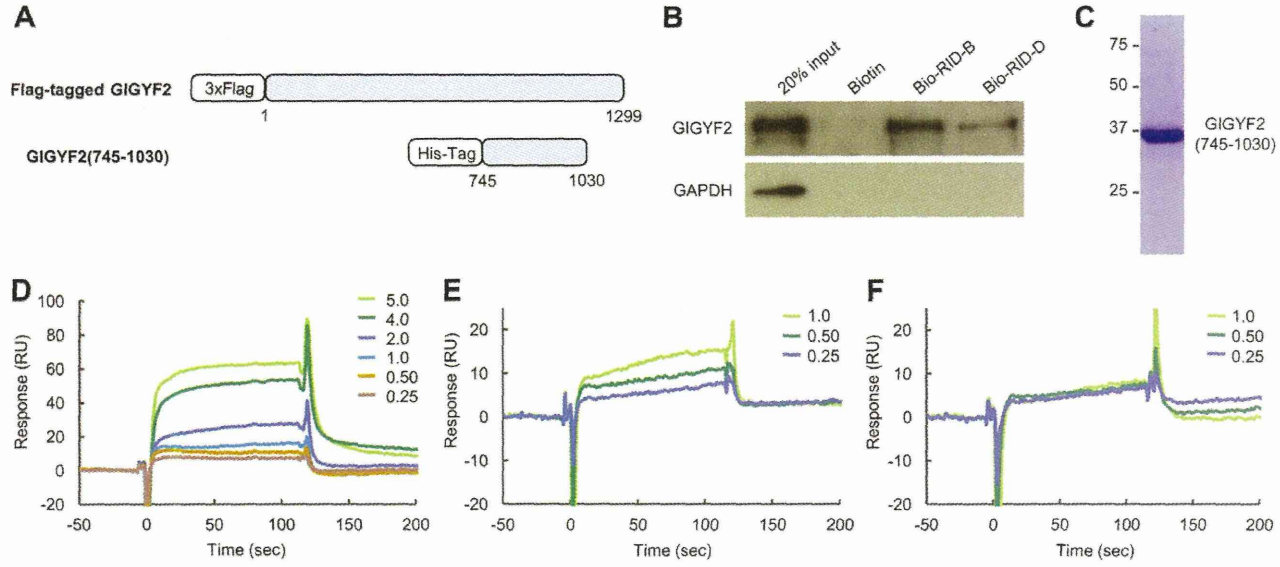

Figure 3. Direct interaction of RID-B with GIGYF2. (A) Schematic representation of the engineered full length or truncated GIGYF2 protein. (B) Interaction of RID-B or RID-D with Flag-tagged GIGYF2. Bio-RID-B, Bio-RID-D or biotin was fixed onto avidin beads and then incubated with cell extracts containing GIGYF2. After extensive washing, the bound GIGYF2 was detected by Western blot analysis. (C) Purified recombinant GIGYF2(745–1030). Recombinant GIGYF2(745–1030) from a bacterial expression system was purified to apparent homogeneity. The purity of the GIGYF2(745–1030) preparation was confirmed by SDS–PAGE analysis followed by staining with CBB. (D–F) A sensorgram obtained from SPR analysis between biotinylated ridaifen derivative and GIGYF2(745–1030). Bio-RID-B (D, E) or Bio-RID-D (F) was immobilized on a SA sensor chip. Solutions of purified GIGYF2(745–1030) at various concentrations (from top to bottom: 5.0, 4.0, 2.0, 1.0, 0.5 or 0.25 μM) was injected over the surface of the sensor chip. The binding responses (in RU) were recorded as a function of time (in sec). The estimated K_D value of interaction between RID-B and GIGYF2(745–1030) was 186 nM.

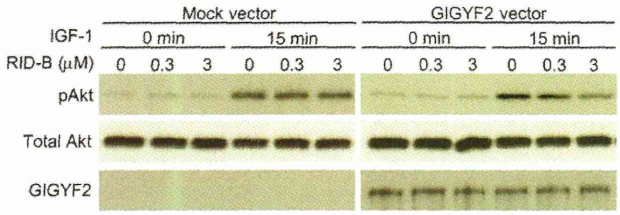

Figure 4. Effect of RID-B on the Akt phosphorylation in GIGYF2-overexpressing cells. HEK293T cells were transiently transfected with mock empty vector or Flag-GIGYF2 expression vector, and were serum-depleted for 20 h. Cells were then treated with 0, 0.3 or 3 μM of RID-B for 4 h followed by stimulation with IGF-1 for 0 or 15 min. Each protein was detected by Western blot analysis using a specific antibody. The data is a representative example from three independent experiments.

3. Conclusion

Our investigations have identified a small molecule that targets GIGYF2, which is involved in the PI3K/Akt signaling pathway and is up-regulated in breast cancer cells where Akt is highly phosphorylated. We employed a T7 phage display screen to identify RID-B-binding protein, a derivative of tamoxifen. Pull-down assay and SPR analysis confirmed the selective interaction between RID-B and GIGYF2. We also demonstrated that RID-B reduces the phosphorylation level of Akt in cells overexpressing GIGYF2. Taken together, our results show that RID-B directly binds to GIGYF2 and reduces the phosphorylation level of Akt at Ser473. Thus, binding of RID-B to GIGYF2 and subsequent reduction of Akt phosphorylation might explain the ER-independent anti-breast cancer activity of RID-B. Furthermore, RID-B and its analogs, as well as being valuable tools for investigating the molecular function of GIGYF2, could be important in the development of novel anti-breast cancer chemotherapy drugs.

4. Materials and methods

4.1. Chemistry

All reagents were purchased from Tokyo Kasei Kogyo Co., Ltd (TCI, Tokyo, Japan), Kanto Chemical Co., Inc. (Tokyo, Japan) or Sigma–Aldrich (St. Louis, MO), and used without further purification. 1-[3-(Benzyloxy)phenyl]propanone (**2**) was prepared from 3-benzyloxybenzaldehyde (Sigma–Aldrich) according to the literature method.[35–37] 2-Methyl-6-nitrobenzoic anhydride (MNBA) was purchased from Tokyo Kasei Kogyo Co., Ltd (M1439).

All melting points are uncorrected. ^{1}H and ^{13}C NMR spectra were recorded with chloroform (in chloroform-*d*) or methanol (in methanol-d_4) as an internal standard. Column chromatography was performed on silica gel 60 (Merck, Darmstadt, Germany). Thin layer chromatography was performed on Wakogel B5F. Unless otherwise stated, all reactions were carried out under an atmosphere of argon using dried glassware. Ammoniacal chloroform was prepared from 28% aqueous ammonia by ammonia extraction with chloroform.

4.2. Compounds

RID-B was synthesized chemically as described in previous reports.[8,9]

4.3. Antibodies

The following primary antibodies were used: rabbit polyclonal anti-GIGYF2 (H-95, Santa Cruz Biotechnology, Santa Cruz, CA), mouse monoclonal anti-GAPDH (6C5, Santa Cruz Biotechnology), rabbit polyclonal anti-Akt (Cell Signaling Technology, Tokyo, Japan), rabbit polyclonal anti-phospho-Akt (Ser473; Cell Signaling Technology).

4.4. Synthesis of Bio-RID-B and Bio-RID-D

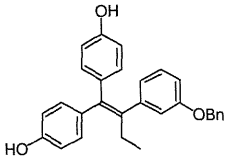

3

4.4.1. 2-[3-(Benzyloxy)phenyl]-1,1-bis(4-hydroxyphenyl)-1-butene (3)

To a suspension of zinc powder (15.8 g, 242 mmol) in THF (30 mL) at −10 °C was added titanium(IV) chloride (12.0 mL, 109 mmol). The reaction mixture was diluted with THF (20 mL) and refluxed at 90 °C (bath temperature) for 2 h and then a mixture of 4,4′-dihydroxybenzophenone (**1**) (12.3 g, 57.3 mmol) and 1-[3-(benzyloxy)phenyl]propanone (**2**) (4.30 g, 17.9 mmol) in THF (60 mL) was added to the mixture at 0 °C. After the reaction mixture had been refluxed at 90 °C (bath temperature) for 2 h in the dark, 10% aqueous potassium carbonate was added to the mixture at 0 °C in the light. The mixture was filtered through a short pad of Celite with ethyl acetate, and the filtrate was extracted with ethyl acetate. The organic layer was washed with brine, and dried over sodium sulfate. After filtration of the mixture and evaporation of the solvent, the crude product was purified by column chromatography on silica gel (eluant; hexane/ethyl acetate = 2:1) to afford **3** (7.09 g, 94%) as a colorless solid: mp: 153–156 °C; IR (KBr): 3402, 3039, 2962, 1589, 1504, 1234 cm^{-1}; ^1H NMR (CD_3OD): δ 7.36–7.26 (5H, m, Ar), 7.08–6.95 (1H, m, Ar), 7.02 (2H, d, J = 8.5 Hz, Ar), 6.76 (2H, d, J = 8.5 Hz, Ar), 6.73–6.67 (3H, m, Ar), 6.67 (2H, d, J = 9.0 Hz, Ar), 6.45 (2H, d, J = 9.0 Hz, Ar), 4.86 (2H, s, Bn), 2.46 (2H, q, J = 7.5 Hz, 3-H), 0.90 (3H, t, J = 7.5 Hz, 4-H); ^{13}C NMR (CD_3OD): δ 159.8, 157.2, 156.4, 145.6, 141.3, 140.1, 138.8 (Ar), 136.4 (1), 136.3 (2), 132.9, 131.6, 130.7, 129.8, 129.4, 128.7, 128.6, 123.5, 117.9, 116.1, 115.8, 115.2, 114.1 (Ar), 71.0 (Bn), 29.7 (3), 14.0 (4); HR MS: calcd for $C_{29}H_{26}O_3Na$ ($M+Na^+$) m/z 445.1774, found 445.1780.

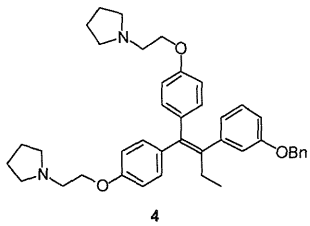

4

4.4.2. 2-[3-(Benzyloxy)phenyl]-1,1-bis{4-[2-(pyrrolidin-1-yl)ethoxy]phenyl}-1-butene (4)

To a solution of **3** (208 mg, 0.493 mmol) in DMF (4.93 mL) at 0 °C was added 60% sodium hydride (dispersion in paraffin liquid, 118 mg, 2.96 mmol). The reaction mixture was stirred for 15 min at 50 °C and then 1-(2-chloroethyl)pyrrolidine hydrochloride (278 mg, 1.63 mmol) was added in portions at room temperature. After the reaction mixture had been stirred for 3 h at 50 °C, saturated aqueous ammonium chloride was added at 0 °C. The mixture was extracted with dichloromethane, and the organic layer was washed with water and brine, and then dried over sodium sulfate. After filtration of the mixture and evaporation of the solvent, the crude product was purified by column chromatography on silica (eluant; ammoniacal chloroform/methanol = 9:1) to afford **4** (267 mg, 88%) as a pale yellow oil: IR (neat): 2962, 1604, 1512, 1242, 1041 cm^{-1}; ^1H NMR ($CDCl_3$): δ 7.40–7.28 (5H, m, Ar), 7.15–7.04 (3H, m, Ar), 6.91–6.70 (7H, m, Ar), 6.59–6.55 (2H, m, Ar), 4.88 (2H, s, Bn), 4.12 (2H, t, J = 6.0 Hz, OCH_2), 3.97 (2H, t, J = 6.0 Hz, OCH_2), 2.91 (2H, t, J = 6.0 Hz, NCH_2), 2.81 (2H, t, J = 6.0 Hz, NCH_2), 2.66–2.54 (8H, m, pyrrolidinyl 2-H), 2.46 (2H, q, J = 7.2 Hz, 3-H), 1.84–1.75 (8H, m, pyrrolidinyl 3-H), 0.93 (3H, t, J = 7.2 Hz, 4-H); ^{13}C NMR ($CDCl_3$): δ 158.3, 157.5, 156.7, 144.0, 140.7, 137.9, 137.1 (Ar), 136.2 (1), 135.8 (2), 131.7, 130.5, 129.6, 128.7, 128.4, 127.7, 127.4, 122.5, 116.3, 114.4, 114.0, 113.3, 112.7 (Ar), 69.8 (Bn), 66.9, 66.7 (OCH_2), 55.05, 55.00 (pyrrolidinyl 2-C), 54.64, 54.59 (NCH_2), 28.8 (3), 23.42, 23.38 (pyrrolidinyl 3-C), 13.6 (4); HR MS: calcd for $C_{41}H_{48}N_2O_3Na$ ($M+Na^+$) m/z 639.3557, found 639.3585.

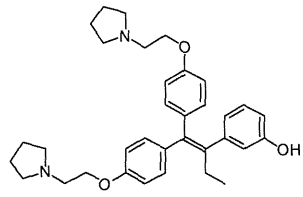

5

4.4.3. 2-(3-Hydroxyphenyl)-1,1-bis{4-[2-(pyrrolidin-1-yl)ethoxy]phenyl}-1-butene (5)

To a solution of **4** (109 mg, 0.177 mmol) in ethyl acetate (5.89 mL) at room temperature under an atmosphere of argon was added palladium on carbon (10% loading, 75.2 mg, 70.7 μmol). The reaction mixture was stirred for 4.5 h at room temperature under an atmosphere of hydrogen (1.0 atm) in the dark, and then transferred to an atmosphere of argon in the light. After filtration of the mixture through a short pad of Celite with ethyl acetate and evaporation of the solvent, the crude product was purified by thin layer chromatography on silica (eluant; ammoniacal chloroform/methanol = 9:1) to afford **5** (93.1 mg, 92%) as a pale yellow oil: IR (neat): 2970, 1604, 1512, 1242, 1049 cm^{-1}; ^1H NMR ($CDCl_3$): δ 7.08 (2H, d, J = 8.5 Hz, Ar), 6.96 (1H, dd, J = 8.0, 8.5 Hz, Ar), 6.84 (2H, d, J = 8.5 Hz, Ar), 6.76 (2H, d, J = 8.5 Hz, Ar), 6.60 (1H, d, J = 7.5 Hz, Ar), 6.53 (2H, dd, J = 2.0, 4.0 Hz, Ar), 6.47 (2H, d, J = 8.5 Hz, Ar), 4.12 (2H, t, J = 6.0 Hz, OCH_2), 3.91 (2H, t, J = 6.5 Hz, OCH_2), 2.93 (2H, t, J = 6.0 Hz, NCH_2), 2.80 (2H, t, J = 6.5 Hz, NCH_2), 2.69–2.62 (4H, m, pyrrolidinyl 2-H), 2.62–2.55 (4H, m, pyrrolidinyl 2-H), 2.39 (2H, q, J = 7.5 Hz, 3-H), 1.85–1.72 (8H, m, pyrrolidinyl 3-H), 0.87 (3H, t, J = 7.5 Hz, 4-H); ^{13}C NMR ($CDCl_3$): δ 157.3, 156.7, 156.5, 144.1, 141.0, 137.3 (Ar), 136.4 (1), 135.9 (2), 131.8, 130.6, 128.9, 121.0, 116.9, 113.9, 113.6, 113.2 (Ar), 66.5, 65.9 (OCH_2), 55.0, 54.9 (pyrrolidinyl 2-C), 54.6, 54.4 (NCH_2), 29.2 (3), 23.3, 23.2 (pyrrolidinyl 3-C), 13.6 (4); HR MS: calcd for $C_{34}H_{43}N_2O_3$ ($M+H^+$) m/z 527.3268, found 527.3247.

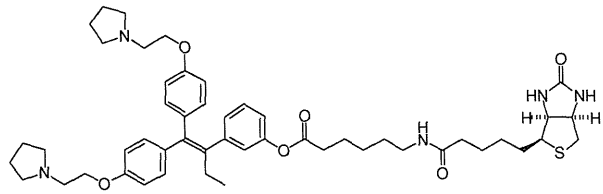

N-Biotinyl-6-aminohexanoic Acid Ridaifen B Ester (Bio-RID-B) (7)

4.4.4. 2-[3-(*N*-Biotinyl-6-aminohexanoyl)phenyl]-1,1-bis{4-[2-(pyrrolidin-1-yl)ethoxy]phenyl}-1-butene (Bio-RID-B) (7)

To a solution of *N*-biotinyl-6-aminohexanoic acid (**6**) (20.0 mg, 56.0 μmol), 2-methyl-6-nitrobenzoic anhydride (MNBA) (23.1 mg, 67.1 μmol), 4-(dimethylamino)pyridine (DMAP) (1.37 mg, 11.2 μmol) and triethylamine (47.0 μL, 0.337 mmol) in dimethylformamide (DMF) (1.41 mL) at 0 °C was added a solution of **5** (35.4 mg, 67.2 μmol) in DMF (0.48 mL). After the reaction mixture had been stirred for 30 min at room temperature, it was concentrated by evaporation of the solvent and then the residue was purified by thin layer chromatography on silica (eluant; ammoniacal chloroform/methanol = 9:1) to afford **7** (33.9 mg, 70%) as a pale yellow oil: IR (neat): 3302, 2931, 1759, 1705, 1643, 1512, 1242, 1049 cm^{-1}; ^1H NMR ($CDCl_3$): δ 7.14–7.10 (3H, m, Ar), 6.92–6.86 (4H, m, Ar), 6.82 (1H, dd, *J* = 2.0, 8.0 Hz, Ar), 6.76 (2H, d, *J* = 9.0 Hz, Ar), 6.57 (2H, d, *J* = 9.0 Hz, Ar), 5.95–5.88 (1H, br m, 7″-NH), 5.83–5.72 (1H, br m, 8″-NH), 5.07–5.00 (1H, br m, 6′-NH), 4.48 (1H, dd, *J* = 5.5, 8.0 Hz, 8″-H), 4.30 (1H, dd, *J* = 4.5, 8.0 Hz, 7″-H), 4.12 (2H, t, *J* = 6.0 Hz, OCH_2), 3.98 (2H, t, *J* = 6.0 Hz, OCH_2), 3.28–3.25 (2H, m, 6′-H), 3.16–3.12 (1H, m, 6″-H), 2.91 (2H, t, *J* = 6.0 Hz, NCH_2), 2.89 (1H, dd, *J* = 5.5, 13.0 Hz, 9″-H), 2.82 (2H, t, *J* = 6.0 Hz, NCH_2), 2.71 (1H, d, *J* = 13.0 Hz, 9″-H), 2.67–2.61 (4H, m, pyrrolidinyl 2-H), 2.61–2.54 (4H, m, pyrrolidinyl 2-H), 2.51 (2H, t, *J* = 7.0 Hz, 2′-H), 2.46 (2H, q, *J* = 7.5 Hz, 3-H), 2.24–2.15 (2H, m, 2″-H), 1.85–1.62 (14H, m, pyrrolidinyl 3-H, 3′-H, 3″-H, 5″-H), 1.58–1.52 (2H, m, 5′-H), 1.47–1.38 (4H, m, 4′-H, 4″-H), 0.93 (3H, t, *J* = 7.5 Hz, 4-H); ^{13}C NMR ($CDCl_3$): δ 173.1 (1″), 172.0 (1′), 163.9 (urea), 157.6, 156.9, 150.4, 144.3, 139.7, 138.6 (Ar), 136.0 (1), 135.4 (2), 131.8, 130.4, 128.6, 127.5, 122.3, 119.0, 114.0, 113.5 (Ar), 67.0, 66.8 (OCH_2), 61.7 (7″), 60.1 (8″), 55.6 (6″), 55.10, 55.07 (pyrrolidinyl 2-C), 54.7, 54.6 (NCH_2), 40.5 (9″), 39.2 (6′), 36.0 (2″), 34.1 (2′), 29.2 (5′), 28.9 (3), 28.2 (4″), 28.1 (5″), 26.3 (4′), 25.7 (3″), 24.4 (3′), 23.45, 23.43 (pyrrolidinyl 3-C), 13.6 (4); HR MS: calcd for $C_{50}H_{68}N_5O_6S$ ($M+H^+$) *m/z* 866.4885, found 866.4842.

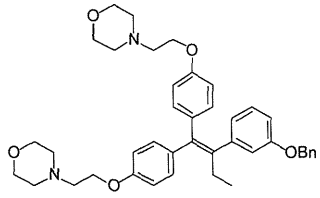

8

4.4.5. 2-[3-(Benzyloxy)phenyl]-1,1-bis{4-[2-(morpholin-4-yl)ethoxy]phenyl}-1-butene (8)

A dispersion of sodium hydride in paraffin liquid (60%, 287 mg, 7.17 mmol) was washed with petroleum ether under an atmosphere of argon. A solution of **3** (501 mg, 1.18 mmol) in DMF (12.0 mL) was then added to the resulting sodium hydride at 0 °C. The reaction mixture was stirred for 15 min at room temperature and then 4-(2-chloroethyl)morpholin hydrochloride (724 mg, 3.89 mmol) was added to the suspension in portions at room temperature. After the reaction mixture had been stirred for 6 h at 50 °C, saturated aqueous ammonium chloride was added at 0 °C. The mixture was extracted with dichloromethane, and the organic layer was washed with water and brine, and dried over sodium sulfate. After filtration of the mixture and evaporation of the solvent, the crude product was purified by column chromatography on silica (eluant; chloroform/methanol = 20:1) to afford **8** (734 mg, 96%) as a pale yellow oil: IR (neat): 2958, 1603, 1507, 1243, 1033 cm^{-1}; ^1H NMR ($CDCl_3$): δ 7.37 (4H, d, *J* = 3.5 Hz, Ar), 7.33–7.30 (1H, m, Ar), 7.13 (2H, d, *J* = 8.5 Hz, Ar), 7.07 (1H, t, *J* = 8.0 Hz, Ar), 6.88 (2H, d, *J* = 8.5 Hz, Ar), 6.77 (2H, d, *J* = 9.0 Hz, Ar), 6.75–6.71 (3H, m, Ar), 6.56 (2H, d, *J* = 8.5 Hz, Ar), 4.89 (2H, s, Bn), 4.13 (2H, t, *J* = 5.5 Hz, OCH_2), 3.98 (2H, t, *J* = 5.5 Hz, OCH_2), 3.75 (4H, t, *J* = 4.5 Hz, morpholinyl OCH_2), 3.69 (4H, t, *J* = 4.5 Hz, morpholinyl OCH_2), 2.82 (2H, t, *J* = 5.5 Hz, NCH_2), 2.72 (2H, t, *J* = 5.5 Hz, NCH_2), 2.59 (4H, t, *J* = 4.5 Hz, morpholinyl NCH_2), 2.52 (4H, t, *J* = 4.5 Hz, morpholinyl NCH_2), 2.45 (2H, q, *J* = 7.5 Hz, 3-H), 0.93 (3H, t, *J* = 7.5 Hz, 4-H); ^{13}C NMR ($CDCl_3$): δ 158.4, 157.4, 156.7, 144.0, 140.9, 137.9, 137.1 (Ar), 136.4 (1), 136.0 (2), 131.8, 130.6, 128.8, 128.5, 127.8, 127.5, 122.6, 116.4, 114.1, 113.4, 112.8 (Ar), 70.0 (Bn), 66.94, 66.89 (OCH_2), 65.7, 65.5 (morpholinyl 2-C), 57.72, 57.67 (morpholinyl 3-C), 54.10, 54.07 (NCH_2), 28.9 (3), 13.6 (4); HR MS: calcd for $C_{41}H_{48}N_2O_5Na$ ($M+Na^+$) *m/z* 671.3455, found 671.3489.

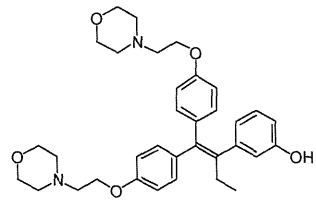

9

4.4.6. 2-(3-Hydroxyphenyl)-1,1-bis{4-[2-(morpholin-4-yl)ethoxy]phenyl}-1-butene (9)

To a solution of **8** (734 mg, 1.13 mmol) in ethyl acetate (32.0 mL) at room temperature under an atmosphere of argon was added palladium on carbon (10% loading, 532 mg, 0.500 mmol). The reaction mixture was stirred for 48 h at room temperature under an atmosphere of hydrogen (1.0 atm) in the dark, and then transferred to an atmosphere of argon in the light. After filtration of the mixture through a short pad of Celite with ethyl acetate and evaporation of the solvent, the residue was diluted with ethyl acetate (32.0 mL) at room temperature under an atmosphere of argon. Palladium on carbon (10% loading, 269 mg, 0.253 mmol) was added to the reaction mixture, which was then stirred for 48 h at room temperature under an atmosphere of hydrogen (1.0 atm) in the dark. The reaction mixture was subsequently transferred to an atmosphere of argon in the light. After filtration of the mixture through a short pad of Celite with ethyl acetate and evaporation of the solvent, the crude product was purified by column chromatography on silica (eluant; chloroform/methanol = 18:1) to afford **9** (507 mg, 80%) as a colorless solid: mp: 51–52 °C; IR (neat): 2959, 1605, 1509, 1243, 1035 cm^{-1}; ^1H NMR ($CDCl_3$): δ 7.11 (2H, d, *J* = 8.5 Hz, Ar), 7.03 (1H, t, *J* = 8.0 Hz, Ar), 6.87 (2H, d, *J* = 10.0 Hz, Ar), 6.77 (2H, d, *J* = 8.5 Hz, Ar), 6.67 (1H, d, *J* = 7.5 Hz, Ar), 6.58–6.53 (4H, m, Ar), 4.13 (2H, t, *J* = 5.5 Hz, OCH_2), 3.97 (2H, t, *J* = 5.5 Hz, OCH_2), 3.74 (4H, t, *J* = 4.5 Hz, morpholinyl OCH_2), 3.70 (4H, t, *J* = 4.5 Hz, morpholinyl OCH_2), 2.82 (2H, t, *J* = 5.5 Hz, NCH_2), 2.71 (2H, t, *J* = 5.5 Hz, NCH_2), 2.60 (4H, t, *J* = 4.5 Hz, morpholinyl NCH_2), 2.53 (4H, t, *J* = 4.5 Hz, morpholinyl NCH_2), 2.43 (2H, q, *J* = 7.5 Hz, 3-H), 0.92 (3H, t, *J* = 7.5 Hz, 4-H); ^{13}C NMR ($CDCl_3$): δ 157.4, 156.7, 155.3, 144.4, 140.7, 137.8 (Ar), 136.4 (1), 135.9 (2), 131.8, 130.6, 129.0, 122.2, 116.7, 114.1, 113.4, 113.1 (Ar), 66.9, 66.8 (OCH_2), 65.7, 65.3 (morpholinyl 2-C), 57.73, 57.65 (morpholinyl 3-C), 54.1, 54.0 (NCH_2), 29.1 (3), 13.6 (4); HR MS: calcd for $C_{34}H_{43}N_2O_5$ ($M+H^+$) *m/z* 559.3166, found 559.3148: calcd for $C_{34}H_{42}N_2O_5Na$ ($M+Na^+$) *m/z* 581.2986, found 581.2978.

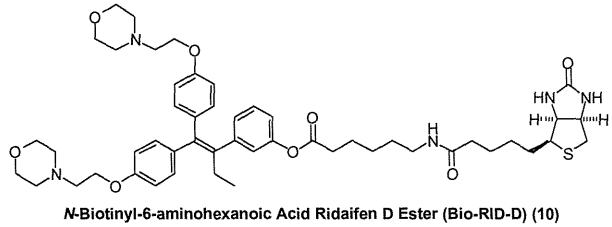

***N*-Biotinyl-6-aminohexanoic Acid Ridaifen D Ester (Bio-RID-D) (10)**

4.4.7. 2-[3-(*N*-Biotinyl-6-aminohexanoyl)phenyl]-1,1-bis{4-[2-(morpholin-4-yl)ethoxy]phenyl}-1-butene (Bio-RID-D) (10)

To a solution of *N*-biotinyl-6-aminohexanoic acid (**6**) (16.0 mg, 44.8 μmol), 2-methyl-6-nitrobenzoic anhydride (MNBA) (18.5 mg, 53.7 μmol), 4-(dimethylamino)pyridine (DMAP) (1.09 mg, 8.92 μmol) and triethylamine (37.4 μL, 0.268 mmol) in dimethylformamide (DMF) (1.34 mL) at 0 °C was added a solution of **9** (30.0 mg, 53.7 μmol) in DMF (0.45 mL). After the reaction mixture had been stirred for 1.5 h at room temperature, it was concentrated by evaporation of the solvent and then the residue was purified by thin layer chromatography on silica (eluant; ammoniacal chloroform/methanol = 9:1) to afford **10** (28.4 mg, 72%) as a pale yellow oil: IR (neat): 3303, 2927, 1765, 1708, 1643, 1507, 1243, 1039 cm^{-1}; ^1H NMR ($CDCl_3$): δ 7.13–7.10 (3H, m, Ar), 6.90–6.75 (7H, m, Ar), 6.55 (2H, d, *J* = 9.0 Hz, Ar), 6.45–6.27 (1H, br m, 7″-NH), 6.18–6.06 (1H, br m, 8″-NH), 5.53–5.36 (1H, br m, 6′-NH), 4.47 (1H, dd, *J* = 4.5, 7.5 Hz, 8″-H), 4.29 (1H, dd, *J* = 5.0, 7.0 Hz, 7″-H), 4.12 (2H, t, *J* = 5.5 Hz, OCH_2), 3.97 (2H, t, *J* = 5.5 Hz, OCH_2), 3.73 (4H, t, *J* = 5.0 Hz, morpholinyl OCH_2), 3.69 (4H, t, *J* = 5.0 Hz, morpholinyl OCH_2), 3.24 (2H, dd, *J* = 6.0, 7.5 Hz, 6′-H), 3.13 (1H, dd, *J* = 4.5, 7.5 Hz, 6″-H), 2.88 (1H, dd, *J* = 4.5, 13.5 Hz, 9″-H), 2.81 (2H, t, *J* = 5.5 Hz, NCH_2), 2.72–2.69 (3H, m, NCH_2, 9″-H), 2.58 (4H, t, *J* = 5.0 Hz, morpholinyl NCH_2), 2.53–2.50 (6H, m, morpholinyl NCH_2, 2′-H), 2.45 (2H, q, *J* = 8.0 Hz, 3-H), 2.19 (2H, t, *J* = 7.0 Hz, 2″-H), 1.76–1.63 (6H, m, 3′-H, 3″-H, 5″-H), 1.57–1.52 (2H, m, 5′-H), 1.47–1.38 (4H, m, 4′-H, 4″-H), 0.93 (3H, t, *J* = 8.0 Hz, 4-H); ^{13}C NMR ($CDCl_3$): δ 173.1 (1″), 172.0 (1′), 163.8 (urea), 157.5, 156.8, 150.5, 144.2, 139.9, 138.5 (Ar), 136.1 (1), 135.5 (2), 131.8, 130.5, 128.7, 127.5, 122.3, 119.0, 114.1, 113.5 (Ar), 66.92, 66.87 (OCH_2), 65.7, 65.6 (morpholinyl 2-C), 61.7 (7″), 60.1 (8″), 57.7, 57.6 (morpholinyl 3-C), 55.6 (6″), 54.1, 54.0 (NCH_2), 40.5 (9″), 39.2 (6′), 36.0 (2″), 34.1 (2′), 29.3 (5′), 28.9 (3), 28.2 (4″), 28.1 (5″), 26.3 (4′), 25.7 (3″), 24.4 (3′), 13.6 (4); HR MS: calcd for $C_{50}H_{68}N_5O_8S$ ($M+H^+$) *m/z* 898.4783, found 898.4740: calcd for $C_{50}H_{67}N_5O_8SNa$ ($M+Na^+$) *m/z* 920.4603, found 920.4615.

4.5. T7 phage display screen

Unless stated otherwise, all manipulations were performed at room temperature. A 10 μM of Bio-RID-B solution was added to a streptavidin-coated 96-well microplate (Nalge Nunc International, Wiesbaden, Germany) and incubated for 1 h. The wells were then blocked with 3% skimmed milk in TBS (25 mM Tris–HCl, 137 mM NaCl, 2.7 mM KCl, pH 7.4) for 1 h. An aliquot of the T7 phage library constructed from cDNA of Jurkat cells was added to each well and the mixture was then incubated for 1 h. After incubation, the wells were washed 10 times with TBST (TBS, 0.1% Tween 20). An elution buffer (TBS, 1% SDS) was then added and the mixture incubated for 15 min to recover the remaining phage particles. In order to amplify the recovered phage particles, each eluate was mixed with a culture of *Esherishia coli* BLT5615 (Merck) at a MOI of 0.001. The cells were then cultured at 37 °C until cell lysis was observed. The resulting solution was used for the next round of biopanning. After four rounds of selection, the eluate was mixed with 1 mL of BLT5615 culture and 10 mL of warmed top agarose and then poured evenly across the surface of an LB/carbenicillin plate. Once the overlay had solidified, the plate was incubated at 37 °C for 3 h in order to allow the formation of phage plaques. A total of 15 plaques were randomly picked and each plaque was suspended in 100 mM NaCl, 6 mM $MgSO_4$, 20 mM Tris–HCl pH 8.0. The DNA sequence of each phage clone was then analyzed as described in a previous report.[16]

4.6. Similarity search

A similarity scores were obtained by FASTA (http://www.ebi.ac.uk/Tools/sss/fasta/).

4.7. Construction of expression vectors

The phage clone displaying 745–1030 a.a. of GIFYF2 was used as a template for the PCR. DNA encoding GIGYF2(745–1030) was amplified using the following primer set: forward, 5′-CATATGG AAATGAGGGCAAAA-3′, and reverse, 5′-CTCGAGTCAACGAGCTCTG TTTGGTTGCT-3′ (underlined bases highlight the restriction endonuclease recognition sites). The PCR product was inserted into pET-28a (+) (Merck) expression vector in-frame with a His-tag at the N-terminus. A full-length GIGYF2 cDNA clone was purchased from Kazusa DNA Research Institute (Gene No. KIAA0642, Chiba, Japan) and the plasmid DNA was used as template for the PCR. The full-length GIGYF2 cDNA was constructed using the following primer set: forward, 5′-GCGGCCGCGGCAGCGGAAACGCAGACACT-3′, and reverse, 5′-GGATCCTCAGTAGTCATCCAACGTCTCGATTTC-3′. The PCR product was inserted into p3xFLAG-CMV-10 (Sigma–Aldrich) expression vector in-frame with 3× FLAG-tag at the N-terminus.

4.8. Expression and purification of recombinant GIGYF2(745–1030)

The engineered GIGYF2(745–1030) expression vector was used to transform *E. coli* Rosetta 2 (DE3)plysS (Merck). These bacteria were grown in LB medium containing 30 μg/mL of kanamycin and 100 μg/mL of chloramphenicol at 37 °C until the OD_{600} reached 0.5 before addition of 1 mM isopropyl thio-β-D-galactoside (IPTG). The cells were then incubated for a further 4 h at 37 °C. After incubation, the cells were harvested and suspended in elution buffer I (50 mM Na_2HPO_4, 5% glycerol, 0.05% Triton X-100, pH 7.2) containing protease inhibitor cocktail (Nacalai Tesque, Kyoto, Japan). The cells were disrupted by sonication and the resulting extract was clarified by centrifugation (17,500g) at 4 °C for 10 min. Solid ammonium sulfate was then gradually added to the clarified cell-free extract to a final concentration of 40% mass/volume. The solution was stirred at 4 °C for 30 min and the final precipitate was pelleted by centrifugation (17,500g) at 4 °C for 10 min and then resuspended in binding buffer I (0.5 M $(NH_4)_2SO_4$, 50 mM Na_2HPO_4, 5% glycerol, 0.05% Triton X-100, pH 7.2). Recombinant GIGYF2(745–1030) was further purified by loading the sample onto a HiTrap Phenyl HP column (1 mL, GE Healthcare UK Ltd, Buckinghamshire, UK) equilibrated in binding buffer I using an FPLC system (GE Healthcare). The bound protein was subsequently eluted with elution buffer I. Fractions containing GIGYF2(745–1030) were pooled and loaded onto a HisTrap HP column (1 mL, GE Healthcare) equilibrated in binding buffer II (7.8 mM Na_2HPO_4, 2.7 mM KCl, 1.5 mM KH_2PO_4, 0.5 M NaCl, 5% glycerol, 0.05% Triton X-100, pH 7.4) using an FPLC system. Finally, bound proteins were eluted using elution buffer II (binding buffer II plus 0.5 M imidazole).

4.9. Surface plasmon resonance assay

SPR analysis was performed on a Biacore® 3000 (GE Healthcare). The purified GIGYF2(745–1030) was buffer exchanged into PBS (67 mM Na_2HPO_4, 12.5 mM KH_2PO_4, 70 mM NaCl, pH 7.4) and the concentration was quantified using DC protein assay kit (Bio-Rad Laboratories, Hercules, CA). Solutions of bovine serum albumin (BSA) at different concentrations were used as standards for this assay. After immobilization of Bio-RID-B and biotin on an SA sensor chip, appropriate concentrations of GIGYF2(745–1030)

were injected over the flow cells. Binding analyses were carried out in PBS at a flow rate of 20 μL/min at 25 °C. The bulk effects of DMSO were subtracted using reference flow cells. Kinetic parameters were determined by analyzing the data using BIAevaluation 4.1 software (GE Healthcare).

4.10. Western blot analysis

Protein samples were separated by SDS–polyacrylamide gel electrophoresis (SDS–PAGE) and transferred from the gel to a polyvinylidene difluoride membrane (Merck) by electroblotting. After blocking for 1 h, proteins were detected by Western blot using primary antibody at the appropriate dilution and horseradish peroxidase-conjugated anti-rabbit or anti-mouse IgG (GE Healthcare) as the secondary antibody. The chemiluminescence was performed using ECL western blotting detection reagents (GE Healthcare) or ECL prime western blotting detection reagent (GE Healthcare).

4.11. Cell culture and transfection

HEK293T cells were maintained in DMEM (Nacalai Tesque) supplemented with 10% fetal bovine serum (Life Technologies, Carlsbad, CA) and 1% Penicillin–Streptomycin Mixed Solution (Nacalai Tesque) at 37 °C under a humidified atmosphere of 5% CO_2. Transient transfection was performed using the X-tremeGENE HP DNA Transfection Reagent (Roche Diagnostics, Indianapolis, IN) according to the manufacturer's instructions.

4.12. Pull-down assay

Twenty-four hours before transfection, HEK293T cells were seeded at 2.5×10^5 cells per well in 6-well plates. Twenty-four hours after transfection with 1 μg of the Flag-tagged GIGYF2 expression vector, the cells from all the wells were harvested in 200 μL 1% Triton lysis buffer (10 mM Tris–HCl pH 7.4, 5 mM EDTA, 1% Triton X-100, protease inhibitor cocktail). The cell lysate was incubated on ice for 1 h and the soluble fraction was then obtained by centrifugation (17,500*g*) at 4 °C for 30 min. The soluble fraction was subsequently diluted by addition of 0.1% Triton buffer with TBS. Avidin–agarose beads (Sigma–Aldrich) were incubated with 10 μM of Bio-RID-B or DMSO and then washed to remove unbound compounds. A 500 μL aliquot of the diluted soluble fraction was then mixed with the avidin–agarose beads at 4 °C for 4 h. The beads were washed 6 times with wash buffer (0.1% Triton buffer in TBS) and the bound proteins were subsequently eluted with 2× SDS sample buffer (100 mM Tris–HCl pH 6.8, 4% SDS, 20% glycerol, 12% β-mercaptoethanol, bromophenol blue). Samples were incubated at 96 °C for 10 min and analyzed by Western blot using antibodies against GIGYF2 (or GAPDH as a control).

4.13. Analysis of the phosphorylation level of Akt

Twenty-four hours before transfection, HEK293T cells were seeded at 2.5×10^5 cells per well in 6-well plates. The cells were transiently transfected with 1 μg of mock empty vector or Flag-tagged GIGYF2 expression vector. Thirty-six hours after transfection, cells were cultured in serum-free medium for 20 h and then incubated with 0, 0.3 or 3 μM (0.1% DMSO) for 4 h following stimulation with 100 ng/mL of IGF-1 (GenScript USA, Piscataway, NJ) for 0 or 15 min. Cells were harvested in 1% Triton lysis buffer containing protease inhibitor cocktail (EDTA-free) and phosphatase inhibitor cocktail (Thermo Fisher Scientific, Waltham, MA) and then the lysates were placed on ice for 1 h. After centrifugation (17,500*g*) at 4 °C for 30 min, the concentration of supernatant was quantified using DC protein assay kit with BSA standards. The supernatant was diluted to 2 mg/mL with 1% Triton lysis buffer and mixed with an equal volume of 2× SDS sample buffer so that the final protein concentration of the sample was 1 mg/mL. The sample was then incubated at 96 °C for 10 min. The data was analyzed by Western blot using antibodies against Akt, phosphorylated Akt or GIGYF2.

Acknowledgment

This study was partially supported by a Health Labour Sciences Research Grant from the Ministry of Health Labour and Welfare, Japan.

Supplementary data

Supplementary data associated with this article can be found, in the online version, at http://dx.doi.org/10.1016/j.bmc.2012.10.037.

References and notes

1. Dhingra, K. *Invest. New Drugs* **1999**, *17*, 285.
2. Fisher, B.; Costantino, J. P.; Wickerham, D. L.; Redmond, C. K.; Kavanah, M.; Cronin, W. M.; Vogel, V.; Robidoux, A.; Dimitrov, N.; Atkins, J.; Daly, M.; Wieand, S.; Tan-Chiu, E.; Ford, L.; Wolmark, N. *J. Natl. Cancer Inst.* **1998**, *90*, 1371.
3. Mandlekar, S.; Kong, A. N. *Apoptosis* **2001**, *6*, 469.
4. Ferlini, C.; Scambia, G.; Marone, M.; Distefano, M.; Gaggini, C.; Ferrandina, G.; Fattorossi, A.; Isola, G.; Benedetti Panici, P.; Mancuso, S. *Br. J. Cancer* **1999**, *79*, 257.
5. Kang, Y.; Cortina, R.; Perry, R. R. *J. Natl. Cancer Inst.* **1996**, *88*, 279.
6. Catherino, W. H.; Jordan, V. C. *Drug Saf.* **1993**, *8*, 381.
7. Dorssers, L. C.; Van der Flier, S.; Brinkman, A.; van Agthoven, T.; Veldscholte, J.; Berns, E. M.; Klijn, J. G.; Beex, L. V.; Foekens, J. A. *Drugs* **2001**, *61*, 1721.
8. Shiina, I.; Sano, Y.; Nakata, K.; Kikuchi, T.; Sasaki, A.; Ikekita, M.; Hasome, Y. *Bioorg. Med. Chem. Lett.* **2007**, *17*, 2421.
9. Shiina, I.; Sano, Y.; Nakata, K.; Kikuchi, T.; Sasaki, A.; Ikekita, M.; Nagahara, Y.; Hasome, Y.; Yamori, T.; Yamazaki, K. *Biochem. Pharmacol.* **2008**, *75*, 1014.
10. Nagahara, Y.; Shiina, I.; Nakata, K.; Sasaki, A.; Miyamoto, T.; Ikekita, M. *Cancer Sci.* **2008**, *99*, 608.
11. Sche, P. P.; McKenzie, K. M.; White, J. D.; Austin, D. *J. Chem. Biol.* **1999**, *6*, 707.
12. Smith, G. P.; Petrenko, V. A. *Chem. Rev.* **1997**, *97*, 391.
13. Takakusagi, Y.; Takakusagi, K.; Sugawara, F.; Sakaguchi, K. *Expert Opin. Drug Discov.* **2010**, *5*, 361.
14. Manita, D.; Toba, Y.; Takakusagi, Y.; Matsumoto, Y.; Kusayanagi, T.; Takakusagi, K.; Tsukuda, S.; Takada, K.; Kanai, Y.; Kamisuki, S.; Sakaguchi, K.; Sugawara, F. *Bioorg. Med. Chem.* **2011**, *19*, 7690.
15. Matsumoto, Y.; Shindo, Y.; Takakusagi, Y.; Takakusagi, K.; Tsukuda, S.; Kusayanagi, T.; Sato, H.; Kawabe, T.; Sugawara, F.; Sakaguchi, K. *Bioorg. Med. Chem.* **2011**, *19*, 7049.
16. Morohashi, K.; Sahara, H.; Watashi, K.; Iwabata, K.; Sunoki, T.; Kuramochi, K.; Takakusagi, K.; Miyashita, H.; Sato, N.; Tanabe, A.; Shimotohno, K.; Kobayashi, S.; Sakaguchi, K.; Sugawara, F. *PLoS One* **2011**, *6*, e18285.
17. Saitoh, T.; Kuramochi, K.; Imai, T.; Takata, K.; Takehara, M.; Kobayashi, S.; Sakaguchi, K.; Sugawara, F. *Bioorg. Med. Chem.* **2008**, *16*, 5815.
18. Takakusagi, K.; Takakusagi, Y.; Ohta, K.; Aoki, S.; Sugawara, F.; Sakaguchi, K. *Protein Eng Des. Sel.* **2010**, *23*, 51.
19. Takami, M.; Takakusagi, Y.; Kuramochi, K.; Tsukuda, S.; Aoki, S.; Morohashi, K.; Ohta, K.; Kobayashi, S.; Sakaguchi, K.; Sugawara, F. *Molecules* **2011**, *16*, 4278.
20. Miyano, Y.; Tsukuda, S.; Sakimoto, I.; Takeuchi, R.; Shimura, S.; Takahashi, N.; Kusayanagi, T.; Takakusagi, Y.; Okado, M.; Matsumoto, Y.; Takakusagi, K.; Takeuchi, T.; Kamisuki, S.; Nakazaki, A.; Ohta, K.; Miura, M.; Kuramochi, K.; Mizushina, Y.; Kobayashi, S.; Sugawara, F.; Sakaguchi, K. *Bioorg. Med. Chem.* **2012**, *20*, 3985.
21. Ajiro, M.; Katagiri, T.; Ueda, K.; Nakagawa, H.; Fukukawa, C.; Lin, M. L.; Park, J. H.; Nishidate, T.; Daigo, Y.; Nakamura, Y. *Int. J. Oncol.* **2009**, *35*, 673.
22. Giovannone, B.; Lee, E.; Laviola, L.; Giorgino, F.; Cleveland, K. A.; Smith, R. J. *J. Biol. Chem.* **2003**, *278*, 31564.
23. Mukaiyama, T. *Angew. Chem., Int. Ed.* **1977**, *16*, 817.
24. Yu, D. D.; Forman, B. M. *J. Org. Chem.* **2003**, *68*, 9489.
25. Shiina, I.; Ibuka, R.; Kubota, M. *Chem. Lett.* **2002**, *31*, 286.
26. Shiina, I.; Kubota, M.; Oshiumi, H.; Hashizume, M. *J. Org. Chem.* **2004**, *69*, 1822.
27. Shiina, I.; Fukui, H.; Sasaki, A. *Nat. Protoc.* **2007**, *2*, 2312.

28. 1-[3-(Benzyloxy)phenyl]propanone (**2**) was prepared from 3-benzyloxybenzaldehyde according to the literature method. See the references in the experimental Section 4.1.
29. Wilchek, M.; Bayer, E. A. *Methods Enzymol.* **1990**, *184*, 123.
30. Elia, G. *Proteomics* **2008**, *8*, 4012.
31. Ajiro, M.; Nishidate, T.; Katagiri, T.; Nakamura, Y. *Int. J. Oncol.* **2010**, *37*, 1085.
32. Alessi, D. R.; Andjelkovic, M.; Caudwell, B.; Cron, P.; Morrice, N.; Cohen, P.; Hemmings, B. A. *EMBO J.* **1996**, *15*, 6541.
33. Scheid, M. P.; Marignani, P. A.; Woodgett, J. R. *Mol. Cell. Biol.* **2002**, *22*, 6247.
34. Yang, J.; Cron, P.; Thompson, V.; Good, V. M.; Hess, D.; Hemmings, B. A.; Barford, D. *Mol. Cell* **2002**, *9*, 1227.
35. Cheng, H. M.; Casida, J. E. *J. Agric. Food Chem.* **1973**, *21*, 1037.
36. Rastogi, S. N.; Anand, N.; Gupta, P. P.; Sharma, J. N. *J. Med. Chem.* **1973**, *16*, 797.
37. Maguire, J. H.; Kraus, B. L.; Butler, T. C.; Dudley, K. H. *Drug Metab. Dispos.* **1981**, *9*, 393.

Journal of Medicinal Chemistry

Article

pubs.acs.org/jmc

Total Synthesis of AMF-26, an Antitumor Agent for Inhibition of the Golgi System, Targeting ADP-Ribosylation Factor 1

Isamu Shiina,*[,†] Yuma Umezaki,[†] Yoshimi Ohashi,[‡] Yuta Yamazaki,[†] Shingo Dan,[‡] and Takao Yamori[‡]

[†]Department of Applied Chemistry, Faculty of Science, Tokyo University of Science, 1-3 Kagurazaka, Shinjuku-ku, Tokyo 162-8601, Japan

[‡]Division of Molecular Pharmacology, Cancer Chemotherapy Center, Japanese Foundation for Cancer Research, 3-8-31 Ariake, Koto-ku, Tokyo 135-8550, Japan

Supporting Information

ABSTRACT: An effective method for the total synthesis of **1** (AMF-26), a potentially promising new anticancer drug that disrupts the Golgi system by inhibiting the ADP-ribosylation factor 1 (Arf1) activation, has been developed for the first time. The construction of the chiral linear precursor (a key to the synthesis) was achieved by the asymmetric aldol reaction followed by the computer-assisted predictive stereoselective intramolecular Diels–Alder reaction. The global antitumor activity of the totally synthetic **1** against a variety of human cancer cells was assessed using a panel of 39 human cancer cell lines (JFCR39), and it was shown that the synthetic **1** strongly inhibited the growth of several cancer cell lines at concentrations of less than 0.04 μM. Biological assays of novel derivatives, **26** and **31**, which have different side-chains at the C-4 positions in the $\Delta^{1,2}$-octalin backbone, disclosed the importance of the suitable structure of the side-chain containing conjugated multidouble bonds.

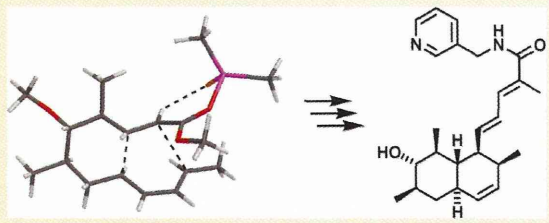

INTRODUCTION

(2*E*,4*E*)-5-((3*S*,4*S*,4a*S*,5*S*,6*S*,7*R*,8a*R*)-3,4,4a,5,6,7,8,8a-Octahydro-6-hydroxy-3,5,7-trimethylnaphthalen-4-yl)-2-methyl-*N*-((pyridin-3-yl)methyl)penta-2,4-dienamide (AMF-26) (**1**)[1] has been semisynthesized from (2*E*,4*E*)-5-((3*S*,4*S*,4a*S*,5*S*,6*S*,7*R*,8a*R*)-3,4,4a,5,6,7,8,8a-octahydro-6-hydroxy-3,5,7-trimethylnaphthalen-4-yl)-2-methylpenta-2,4-dienoic acid (AMF-14) (**2**),[2] a natural product isolated from the genus *Trichoderma* NFS-932 by Nippon Shinyaku Co., Ltd., in 2005 (Figure 1). The

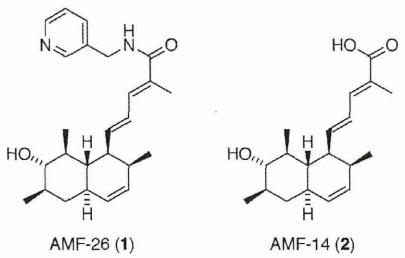

Figure 1. Structures of AMF-26 (**1**) and AMF-14 (**2**).

compound **1** is a potentially promising new anticancer drug lead because its oral administration to female nude mice induced complete regression of human breast cancer BSY-1 xenografts in vivo.[2] It was revealed that **1** induced Golgi disruption, apoptosis, and cancer-cell growth inhibition through a mechanism for preventing the ADP-ribosylation factor 1 (Arf1) activation introduced by Ohashi and Yamori et al.[2] Arf1 has an important role in mediating vesicular transport. Recently, protein–protein interaction, such as the activation of Arf1 by its guanine nucleotide exchange factor (ArfGEF), has become a very attractive new target for providing effective therapeutic agents, including novel anticancer drugs.[3] From computer modeling, it is postulated that **1** binds to the contact surface of the Arf1–Sec7 domain where brefeldin A bound. Brefeldin A was first introduced as the inhibitor of the Arf1–ArfGEF interaction;[4−6] however, brefeldin A has not progressed beyond the preclinical stage of drug development because of its poor bioavailability.[6a,7] Therefore, **1**, a new Golgi inhibitor targeting Arf1 activation, can be one of the first candidates for a new type of medicine for cancer treatment in clinical use. Furthermore, another biological activity of **1**, angiogenesis inhibition of the vascular endothelial growth factor (VEGF) receptor phosphorylation and NF-κB signaling, has been investigated by Watari and Nakamura et al.[8]

In this study, we report the first total synthesis of **1** using the asymmetric aldol reaction for constructing the chiral linear precursor and computer-assisted predictive stereoselective intramolecular Diels–Alder (IMDA) reaction to provide the core structure of the multisubstituted octahydronaphthalene.

TOTAL SYNTHESIS OF AMF-26

Retrosynthetic Analysis of 1 via IMDA Reaction. Scheme 1 outlines our designed asymmetric synthesis of **1**, including the three following notable methodologies: (i) the diastereoselective

Received: September 18, 2012
Published: December 6, 2012

   dx.doi.org/10.1021/jm301695c | *J. Med. Chem.* 2013, 56, 150−159

Scheme 1. Retrosynthetic Analysis of 1

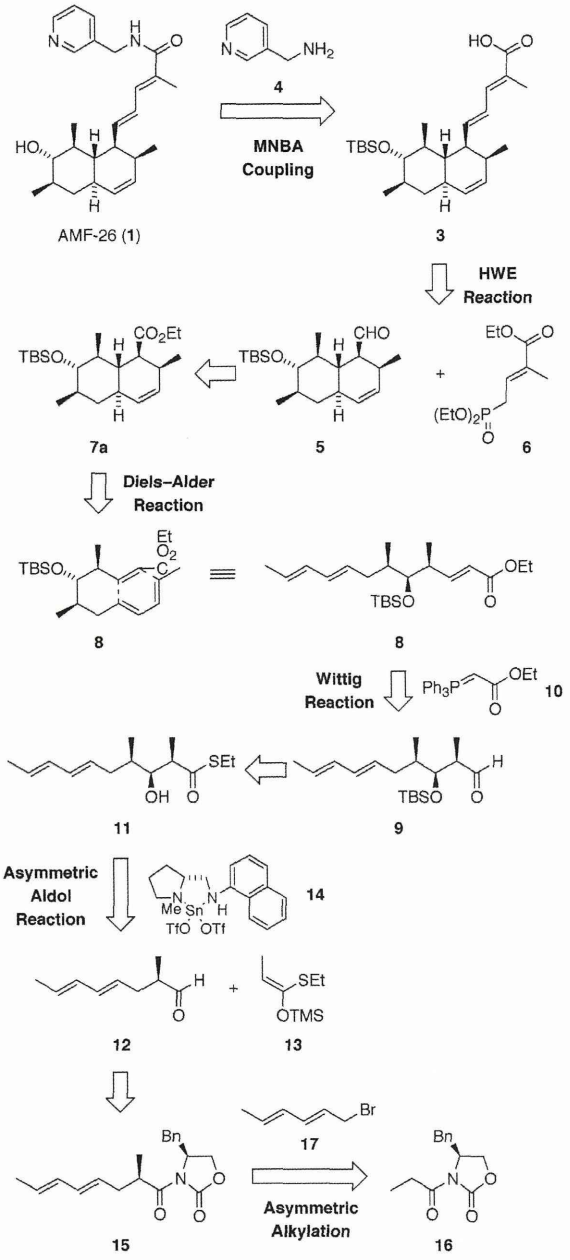

Evans' alkylation[9] of the chiral oxazolidinone **16** with (*E,E*)-1-bromohexa-2,4-diene (**17**) to form a chiral diene **15**, (ii) the enantioselective Mukaiyama aldol reaction[10] of an aldehyde **12** with ketene silyl acetal (KSA) **13** to form an α,β,γ-trisubstituted chiral thioester **11**, and (iii) the diastereoselective IMDA reaction[11] of the chiral linear ester **8** to form octahydronaphthalene **7a**. Other transformations, such as the Wittig reaction of an aldehyde **9** with an ylide **10** to provide an ester **8**, the HWE (Horner–Wadsworth–Emmons) reaction of an aldehyde **5** with phosphate **6** to provide a carboxylic acid **3**, and the MNBA coupling reaction[12] of **3** with 3-pyridylmethylamine (**4**) to afford the corresponding amide, might be successfully carried out for the preparation of the basic skeleton of the target molecule **1** in this plan.

Asymmetric Synthesis of Chiral Linear Ester 8 and Prediction of the Stereoselectivity in the IMDA Reaction of 8M to Form $\Delta^{1,2}$-Octalins 7Ma–d. First, Evans' chiral oxazolidinone **16**[9] was converted into the sodium enolate by the reaction with NaHMDS, followed by the treatment with **17**[13] in the presence of tetrabutylammonium iodide (TBAI) to diastereoselectively form diene **15** (Scheme 2). Removal of the chiral auxiliary

Scheme 2. Preparation of the Key Chiral Linear Ester 8 Intermediate[a]

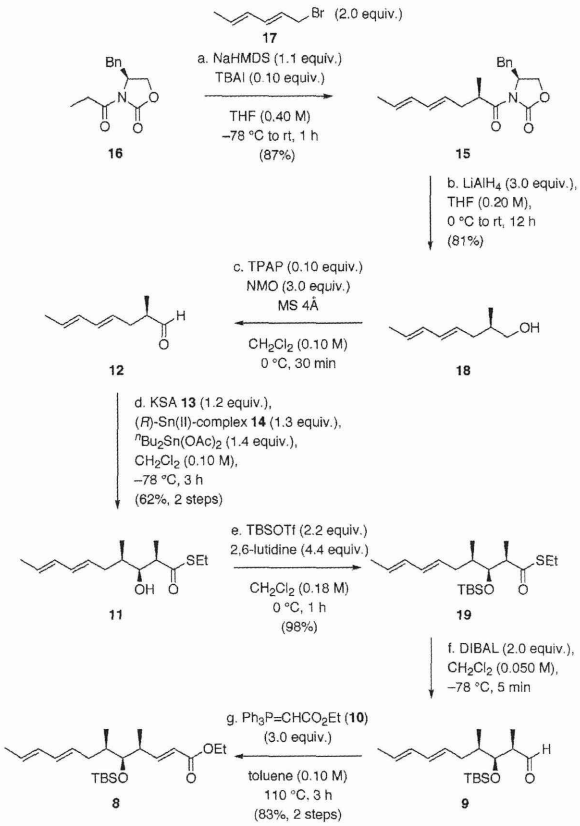

[a]Reagents and conditions: (a) NaHMDS, THF, −78 °C, 15 min, and then bromide **17**, TBAI, rt, 1 h, 87%; (b) $LiAlH_4$, THF, 0 °C to rt, 12 h, 81%; (c) TPAP, NMO, 4-Å molecular sieves, CH_2Cl_2, 0 °C, 30 min; (d) KSA **13**, (*R*)-Sn(II)-complex **14**, $^nBu_2Sn(OAc)_2$, CH_2Cl_2, −78 °C, 3 h, 62% from **18**; (e) TBSOTf, 2,6-lutidine, CH_2Cl_2, 0 °C, 1 h, 98%; (f) DIBAL, CH_2Cl_2, −78 °C, 5 min; (g) $Ph_3P{=}CHCO_2Et$ (**10**), toluene, 110 °C, 3 h, 83% from **19**.

in **15** by reduction with lithium aluminum hydride and the successive oxidation of the primary alcohol **18** using tetrapropylammonium perruthenate (TPAP) afforded the (*E,E*)-dieneal-dehyde **12** in good yield. The enantioselective Mukaiyama aldol reaction[10] of **12** with KSA **13** in the presence of the chiral Sn(II) complex **14** smoothly took place to exclusively provide the desired α,β,γ-trisubstituted thioester **11**. Protection of the free hydroxyl group in **11** and reduction of the resulting *tert*-butyldimethylsiloxy (TBS) ether **19** with diisobutylaluminum hydride (DIBAL) were carried out to afford the chiral aldehyde **9**, and then the sequential treatment of **9** with Wittig reagent

dx.doi.org/10.1021/jm301695c | J. Med. Chem. 2013, 56, 150−159